

# Probing aromatic, hydrophobic, and steric effects on the self-assembly of an amyloid- $\beta$ fragment peptide†

F. Timur Senguen,<sup>a</sup> Naomi R. Lee,<sup>a</sup> Xianfeng Gu,<sup>b</sup> Derek M. Ryan,<sup>a</sup> Todd M. Doran,<sup>a</sup> Elizabeth A. Anderson<sup>a</sup> and Bradley L. Nilsson<sup>\*a</sup>

Received 2nd July 2010, Accepted 8th October 2010

DOI: 10.1039/c0mb00080a

Aromatic amino acids have been shown to promote self-assembly of amyloid peptides, although the basis for this amyloid-inducing behavior is not understood. We adopted the amyloid- $\beta$  16–22 peptide (A $\beta$ (16–22), Ac-KLVFFAE-NH<sub>2</sub>) as a model to study the role of aromatic amino acids in peptide self-assembly. A $\beta$ (16–22) contains two consecutive Phe residues (19 and 20) in which Phe19 side chains form interstrand contacts in fibrils while Phe20 side chains interact with the side chain of Val18. The kinetic and thermodynamic effect of varying the hydrophobicity and aromaticity at positions 19 and 20 by mutation with Ala, Tyr, cyclohexylalanine (Cha), and pentafluorophenylalanine (F<sub>5</sub>-Phe) (order of hydrophobicity is Ala < Tyr < Phe < F<sub>5</sub>-Phe < Cha) was characterized. Ala and Tyr position 19 variants failed to undergo fibril formation at the peptide concentrations studied, but Cha and F<sub>5</sub>-Phe variants self-assembled at dramatically enhanced rates relative to wild-type. Cha mutation was thermodynamically stabilizing at position 20 ( $\Delta\Delta G = -0.2$  kcal mol<sup>-1</sup> relative to wild-type) and destabilizing at position 19 ( $\Delta\Delta G = +0.2$  kcal mol<sup>-1</sup>). Conversely, F<sub>5</sub>-Phe mutations were strongly stabilizing at both positions ( $\Delta\Delta G = -1.3$  kcal mol<sup>-1</sup> at 19,  $\Delta\Delta G = -0.9$  kcal mol<sup>-1</sup> at 20). The double Cha and F<sub>5</sub>-Phe mutants showed that the thermodynamic effects were additive ( $\Delta\Delta G = 0$  kcal mol<sup>-1</sup> for Cha19,20 and  $-2.1$  kcal mol<sup>-1</sup> for F<sub>5</sub>-Phe19,20). These results indicate that sequence hydrophobicity alone does not dictate amyloid potential, but that aromatic, hydrophobic, and steric considerations collectively influence fibril formation.

## Introduction

The self-assembly of peptides and proteins into cross- $\beta$  amyloid structures is a defining characteristic of protein misfolding pathologies including Alzheimer's disease, Parkinson's disease, type 2 diabetes, and prion encephalopathies.<sup>1,2</sup> Amyloid structures are not only associated with disease states, but also exist as evolutionarily conserved motifs with defined biological function.<sup>3,4</sup> There is growing interest in exploiting peptide self-assembly phenomena for the development of novel functional structures with applications in biomedicine, energy, and materials.<sup>5–10</sup> Significant effort is currently directed at understanding the biophysical constraints that contribute to amyloid formation and stability. These efforts are motivated by the need to modulate the formation of pathological amyloid *in vivo* as potential therapeutic strategies for amyloid disorders in addition to the development of beneficially bioactive amyloid materials.<sup>11</sup>

The self-assembly of amyloid peptides is governed by non-covalent interactions, including hydrogen bonds, coulombic

interactions and hydrophobic effects.<sup>12–15</sup> Aromatic  $\pi$ - $\pi$  interactions<sup>16</sup> have been proposed to play a critical role in the formation of amyloid cross- $\beta$  assemblies by mediating favorable early molecular recognition events that direct self-assembly.<sup>17</sup> Aromatic interactions are known to stabilize  $\alpha$ -helices<sup>18</sup> and  $\beta$ -sheets<sup>19</sup> in discrete protein structures, and the abundance of otherwise rare aromatic amino acids in core regions of amyloid peptides implies a role for  $\pi$ - $\pi$  interactions in peptide self-assembly as well.<sup>17,20</sup>

Mutational analyses of amyloid peptides in which aromatic  $\rightarrow$  Ala substitutions arrest self-assembly support a prominent role for  $\pi$ - $\pi$  interactions in these processes.<sup>21,22</sup> In addition, many effective inhibitors of amyloid formation target molecular recognition events involving aromatic amino acids, providing additional evidence that  $\pi$ - $\pi$  interactions are of some importance in early self-assembly events.<sup>17,23–26</sup> However, it has been shown that the presence of aromatic residues in amyloidogenic sequences is not strictly a requirement for self-assembly.<sup>19,27–29</sup> Mutational studies of amyloidogenic peptides that utilize more conservative aromatic  $\rightarrow$  Leu mutations (relative to aromatic  $\rightarrow$  Ala) indicate that Leu-containing variants readily self-assemble, although at attenuated rates relative to the parent aromatic sequences.<sup>27,28</sup> The slower rate of aggregation in these types of variants has been shown to be more consistent with differences in hydrophobicity and  $\beta$ -sheet propensity rather than the loss of attractive  $\pi$ - $\pi$  interactions.<sup>15,30</sup> In fact, it has been suggested that the high amyloidogenicity of aromatic amino acids

<sup>a</sup> Department of Chemistry, University of Rochester, Rochester, NY, 14627-0216, USA. E-mail: nilsson@chem.rochester.edu; Fax: +1 585-276-0205; Tel: +1 585-276-3053

<sup>b</sup> School of Pharmacy, Fudan University, 826 Zhangheng Road, Shanghai, China 201301

† Electronic supplementary information (ESI) available: Peptide characterization data, reverse HPLC sedimentation assays, concentration curves, concentration curve determination method. See DOI: 10.1039/c0mb00080a

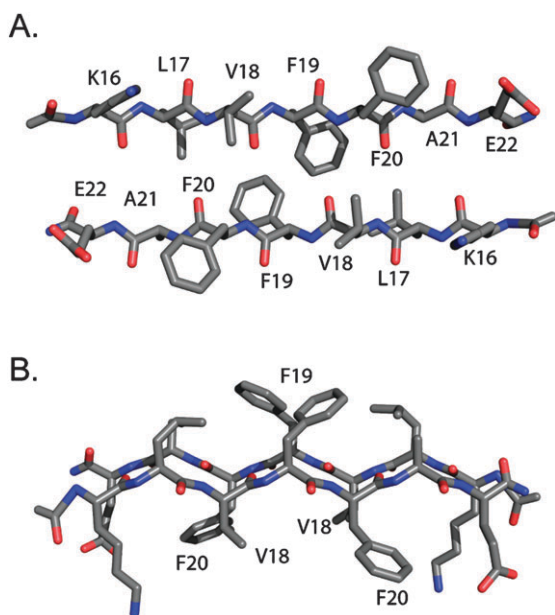


**Fig. 1** The current model of strand orientation within  $\beta$ -sheets of fibrils derived from the  $A\beta(16-22)$  fragment. (A) View perpendicular to fibril axis. (B) View along fibril axis.

(Phe, Trp, and Tyr) can be accounted for entirely by hydrophobicity and secondary structural propensity without invoking  $\pi$ - $\pi$  interactions.<sup>31</sup> Additional study to elucidate the relative contributions of  $\pi$ - $\pi$  interactions in peptide self-assembly is necessary.

To probe the importance of aromatic amino acids in peptide self-assembly we chose to investigate the role of the Phe-Phe motif in the Alzheimer's disease amyloid- $\beta$  peptide ( $A\beta$ ). The Phe-Phe motif is present in other amyloidogenic peptides, including serum amyloid protein, and additionally it has been found that the peptide dimer, Phe-Phe, can independently form ordered superstructures.<sup>32-34</sup> We chose the hydrophobic core peptide of amyloid- $\beta$ ,  $A\beta(16-22)$ , as a model to probe aromatic effects.<sup>35-41</sup> At neutral pH, this peptide is known to form amyloid fibers by adopting an antiparallel strand-packing mode within the  $\beta$ -sheets.<sup>35,39,42,43</sup> When assembled into antiparallel  $\beta$ -sheets, the side chain of the central Phe residues at position 19 forms inter-strand contacts with neighboring Phe19 side chains (Fig. 1). This cross-strand contact may involve specific  $\pi$ - $\pi$  interactions.<sup>39</sup> Conversely, the flanking Phe20 side chain interacts cross-strand with the Val18 side chain. Changes in hydrophobicity and aromaticity at these positions will elucidate the importance of the central aromatic core in the self-assembly process, providing insight into  $\pi$ - $\pi$ , hydrophobic, and steric effects on fibril formation.

Nonnatural amino acids facilitate a more focused comparison of aromatic and hydrophobic effects since residues can be utilized that have aromatic or nonaromatic decoration and are more hydrophobic than either Trp or Phe without greatly disturbing the general carbon skeleton.<sup>44</sup> Early studies from our group involving the incorporation of the highly hydrophobic, nonaromatic cyclohexylalanine (Cha) ( $\pi_{\text{Cha}} = 2.72$ ,  $\pi_{\text{Phe}} = 1.71$ )<sup>45</sup> into amphipathic self-assembling peptides suggested enhanced self-assembly propensities for Cha-containing peptides, although the self-assembly of the target (XKXE)<sub>n</sub>

repeats was so rapid that comparative kinetic or thermodynamic analyses could not be conducted.<sup>46</sup> Pentafluorophenylalanine ( $F_5$ -Phe), another interesting nonnatural amino acid, is intermediate in hydrophobicity relative to Phe and Cha ( $\pi_{F_5\text{-Phe}} = 2.12$ ) while maintaining aromatic character.<sup>47,48</sup> The effect on self-assembly of increasing hydrophobicity at the central Phe-Phe core serves as a complementary approach to previous studies that incorporate less hydrophobic functionality.

We prepared nine variants of  $A\beta(16-22)$  to probe hydrophobic and aromatic effects in self-assembly involving the Phe-Phe motif. The native sequence (wild-type, peptide 1) and two less hydrophobic sequences, incorporating Ala (nonaromatic) and Tyr (aromatic) at position 19 (peptides 2 and 3, respectively), were synthesized. Two sequences incorporate amino acids with greater hydrophobicity at position 19 relative to the native sequence,  $F_5$ -Phe19 (peptide 4) and Cha19 (peptide 5) and two sequences include the same nonnatural amino acids at the flanking position (Phe20) (peptides 6 and 7). Finally, double mutants substituting both the central and flanking position with  $F_5$ -Phe (peptide 8) and Cha (peptide 9) were prepared. The Phe  $\rightarrow$  Cha variants remove possible  $\pi$ - $\pi$  interactions in the fibrils while most dramatically increasing the sequence hydrophobicity. The Phe  $\rightarrow$   $F_5$ -Phe mutants allow for  $\pi$ - $\pi$  interactions but are intermediate in hydrophobicity between the Phe and Cha peptides.

We hypothesized that increasing hydrophobicity would enhance self-assembly propensity, and that this effect would be exaggerated at position 19, where 19-19 cross-strand interactions occur.<sup>35,39,43</sup> The lack of possible  $\pi$ - $\pi$  interactions in peptides 5 and 9 will also provide interesting insight into the role of aromatic interactions in respect to the Phe-Phe motif.

## Results and discussion

### Peptide synthesis and hydrophobicity

The  $A\beta(16-22)$  variants were prepared by solid phase peptide synthesis as the *N*-acetyl, C-terminal amide sequences. HPLC analysis confirmed the predicted hydrophobicity of the peptides (Cha  $\geq$   $F_5$ -Phe > Phe > Tyr > Ala) based on increasing retention times using identical stationary and mobile phase conditions (Fig. S2-S10, ESI<sup>†</sup>). This order of sequence hydrophobicity of the model peptides was further confirmed by simultaneous HPLC co-injection in order to avoid experimental inconsistencies with HPLC gradients, injection times, *etc.* The peaks were analyzed by mass spectrometry, and the retention times followed the predicted order based on hydrophobicity (see ESI<sup>†</sup>, Fig. S11-S17, Tables S2-S4).

### Effect of sequence hydrophobicity at position 19

The self-assembly behavior of these peptides was characterized using Wetzel's HPLC sedimentation assay.<sup>49</sup> Disaggregated peptides were incubated at 37 °C (55  $\mu$ M peptide, pH 7.6, 5% DMSO/phosphate buffered saline). Periodically, aliquots of each self-assembly reaction were removed and aggregates were sedimented by ultracentrifugation followed by determination of remaining monomer concentration by correlation to an

HPLC concentration curve. Sedimentation by ultracentrifugation at high spin rates (see Experimental section) has been shown to remove fibrils and lower order, oligomeric, aggregates.<sup>49</sup> Dynamic light scattering analysis of supernatant following sedimentation and removal of aggregates showed no evidence of remaining oligomeric structures, giving strong confidence that the dominant species in solution following sedimentation are indeed monomeric. It should be noted, however, that dynamic low order aggregates (dimer, trimer, *etc.*) may be present and that HPLC sedimentation protocols cannot accurately account for these species. The observation of decreasing monomer concentration in solution as a function of time allows approximation of relative self-assembly kinetics. In addition, peptide self-assembly proceeds to a final dynamic equilibrium that can be characterized by determining the critical concentration of peptide monomer ( $C_r$ ). At equilibrium an association constant ( $K_a$ ) for the addition of a single molecule of monomeric peptide to a fibril can be determined from  $C_r$  by the relationship shown in eqn (2) (Experimental).<sup>49</sup> This is reflective of the final equilibrium state: fibril<sub>n</sub> + monomer  $\leftrightarrow$  fibril<sub>n+1</sub>. The characteristic  $K_a$  values for each peptide can be subsequently used to determine free energies for this interaction ( $\Delta G$ ), providing relative thermodynamic comparisons of the variants.<sup>49</sup>

The native A $\beta$ (16–22) (wild-type) sequence displayed a  $C_r$  value of  $33 \pm 3 \mu\text{M}$  from a starting concentration of  $55 \mu\text{M}$  (Fig. 2 and Table 1). There was an initial lag phase of 12 h after which self-assembly commenced and continued for  $\sim 14$  days before reaching equilibrium. This equilibrium  $C_r$  value was confirmed by suspending mature fibrils in buffer and observing the increasing concentration of monomer over time. In this experiment, a final monomer concentration of  $32 \mu\text{M}$  was observed at equilibrium (Fig. S1, ESI $\dagger$ ). Attempts to corroborate HPLC sedimentation data by thioflavin T (ThT) fluorescence measurements were precluded by low binding affinity and fluorescence response of ThT to fibrils derived from the A $\beta$  16–22 region (including A $\beta$ (16–22) and A $\beta$ (16–20)), as has been previously observed.<sup>50–52</sup>

Decreasing the hydrophobicity of the amino acid at position 19 inhibited self-assembly relative to the native sequence. Neither the Ala19 nor the Tyr19 variants exhibited any evidence of self-assembly at peptide concentrations of  $55 \mu\text{M}$  (Fig. 2A). These peptides remained soluble and monomeric for  $>3$  weeks by HPLC sedimentation analysis (Fig. 2B). The starting concentration of these peptides was increased to  $100 \mu\text{M}$  and still no evidence of self-assembly was observed, indicating that the  $C_r$  for self-assembly of the Ala19 and Tyr19 variants is  $>100 \mu\text{M}$ . Wetzel *et al.* have previously studied the Phe19  $\rightarrow$  Ala mutant of full-length A $\beta$ ; it was found that the  $\Delta\Delta G$  for the self-assembly of this variant was  $1.5 \text{ kcal mol}^{-1}$  relative to wild-type.<sup>53</sup> Based on this precedent, we calculated that the expected  $C_r$  for our Ala19 A $\beta$ (16–22) variant would be at least  $350 \mu\text{M}$ , consistent with our observations that no self-assembly occurs up to  $100 \mu\text{M}$ . Based on these deleterious effects on self-assembly, mutational analyses with Ala and Tyr at position 20 or in both 19 and 20 positions were not explored.

The Cha19 and F<sub>5</sub>-Phe19 variants exhibited significant kinetic enhancement in fibril self-assembly relative to the native peptide (Fig. 2A). While the native Phe19 peptide

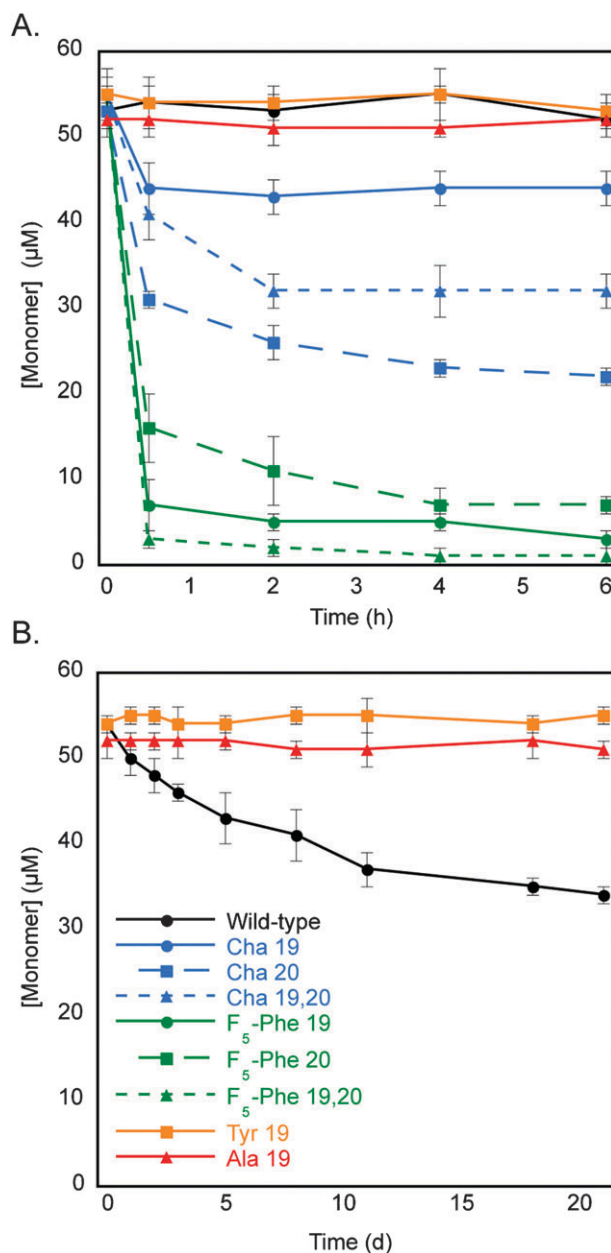


**Fig. 2** HPLC sedimentation data for fibrillization of A $\beta$ (16–22) variants indicating decrease in monomer peptide concentration over time. (A) Short-term (6 h) time course for all variants. (B) Long-term (21 day) time course for wild-type A $\beta$ (16–22) and the Phe19  $\rightarrow$  Ala and Phe19  $\rightarrow$  Tyr variants.

displayed a 12 h lag phase and required weeks to reach equilibrium from a starting concentration of  $55 \mu\text{M}$ , both hydrophobic variants (F<sub>5</sub>-Phe19 and Cha19) assembled to equilibrium within 30 min (Fig. 2A). The relative rates of self-assembly of the F<sub>5</sub>-Phe19 (4) and Cha19 (5) variants could not be effectively differentiated based on HPLC sedimentation analysis. The rapid rate of assembly for these peptides prevented a more detailed kinetic analysis since ThT fluorescence assays were not viable<sup>50</sup> and the rates of self-assembly were sufficiently rapid that HPLC sedimentation protocols did not allow the acquisition of multiple early time points. Efforts to slow self-assembly by reducing the starting

**Table 1** A $\beta$ (16–22) variant peptides and amino acid hydrophobicities for residues at positions 19 and 20

Peptide	Sequence	Variant	$\Pi^a$
1	Ac-KLVFFAE-NH <sub>2</sub>	Native (Phe)	1.71
2	Ac-KLVFAAE-NH <sub>2</sub>	Phe19 → Ala	0.31
3	Ac-KLVYFAE-NH <sub>2</sub>	Phe19 → Tyr	0.96
4	Ac-KLV(F <sub>5</sub> -Phe)FAE-NH <sub>2</sub>	Phe19 → F <sub>5</sub> -Phe	2.12
5	Ac-KLV(Cha)FAE-NH <sub>2</sub>	Phe19 → Cha	2.72
6	Ac-KLVF(F <sub>5</sub> -Phe)AE-NH <sub>2</sub>	Phe20 → F <sub>5</sub> -Phe	2.12
7	Ac-KLVF(Cha)AE-NH <sub>2</sub>	Phe20 → Cha	2.72
8	Ac-KLV(F <sub>5</sub> -Phe)(F <sub>5</sub> -Phe)AE-NH <sub>2</sub>	Phe19,20 → F <sub>5</sub> -Phe	2.12
9	Ac-KLV(Cha)(Cha)AE-NH <sub>2</sub>	Phe19,20 → Cha	2.72

<sup>a</sup> Hydrophobicity of the position 19 and/or 20 amino acid based on water–octanol partition coefficients relative to Gly.<sup>45,47</sup>

concentration or solution temperature were unsuccessful at decelerating the rate of self-assembly sufficiently to observe earlier kinetic time points under the constraints of the HPLC sedimentation assay.

Increasing the sequence hydrophobicity of A $\beta$ (16–22) at position 19 also perturbed the dynamic equilibrium of the self-assembly process as shown by the  $C_r$  values for the Cha19 and F<sub>5</sub>-Phe19 peptides (Fig. 2 and Table 2). The Cha19 variant had a  $C_r$  value of  $44 \pm 3 \mu\text{M}$  and the F<sub>5</sub>-Phe19 peptide reached  $4 \pm 1 \mu\text{M}$  at endpoint. These  $C_r$  values were validated as equilibrium endpoints by monitoring monomer concentrations after suspending mature fibrils in buffer; Cha19 reached  $43 \mu\text{M}$  and F<sub>5</sub>-Phe19 reached  $3 \mu\text{M}$  monomer concentrations in these experiments (Fig. S1, ESI<sup>†</sup>). Increasing sequence hydrophobicity without conserving  $\pi$ – $\pi$  interactions by mutating Phe19 to Cha provides subtle thermodynamic destabilization to fibrils ( $\Delta\Delta G = +0.2 \text{ kcal mol}^{-1}$ ) in the context of this peptide. This unexpected result clearly indicates that the hydrophobic character of amyloidogenic sequences does not entirely control the kinetics and thermodynamics of peptide self-assembly. Conversely, increasing the hydrophobicity and retaining aromaticity at position 19 by using F<sub>5</sub>-Phe resulted in a significant thermodynamic stabilization of self-assembly ( $\Delta\Delta G = -1.3 \text{ kcal mol}^{-1}$ ) despite the lower hydrophobicity of F<sub>5</sub>-Phe relative to Cha. These results do not follow the order predicted by hydrophobicity alone (Cha > F<sub>5</sub>-Phe > Phe); rather, this data may be consistent with a significant energetic contribution for  $\pi$ – $\pi$  interactions in the context of position 19 for this peptide. Alternatively, this data could be consistent with a specific destabilization related to Cha incorporation at position 19.

### Effect of sequence hydrophobicity at position 20

The results of mutating the flanking aromatic residue (Phe20) to F<sub>5</sub>-Phe (6) and Cha (7) mirror those obtained by mutating

the central hydrophobic residue, however the effects are dampened. This is probably due to the fact that the side chain at position 20 interacts with the Val18 side chain in cross-strand pairing (Fig. 1), providing a heterologous contact. This contrasts with position 19 in which side chains participate in homologous cross-strand interactions with neighboring residue 19 side chains. The introduction of the more hydrophobic residues into the flanking position increased the rate of self-assembly dramatically as both variants reach equilibrium within hours rather than weeks as compared to the wild-type peptide. As with the variants at the central position, these peptides aggregate so rapidly that their comparative rates could not be precisely differentiated.

The thermodynamic effects of increased hydrophobicity at position 20 was summarily stabilizing (Table 2), with the Cha20 and F<sub>5</sub>-Phe20 mutants reaching  $C_r$  values of  $22 \pm 1 \mu\text{M}$  and  $7 \pm 1 \mu\text{M}$ , respectively. Suspensions of fibrils as described earlier confirmed these  $C_r$  values at equilibrium ( $21 \mu\text{M}$  for Cha20 and  $7 \mu\text{M}$  for F<sub>5</sub>-Phe20, Fig. S1, ESI<sup>†</sup>). These critical concentrations translate to thermodynamic stabilizations relative to the wild-type ( $\Delta\Delta G$ ) of  $-0.2 \pm 0.1 \text{ kcal mol}^{-1}$  and  $-0.9 \pm 0.1 \text{ kcal mol}^{-1}$ , respectively, and demonstrate that increasing the hydrophobicity at this flanking position generally stabilizes the resulting fibrils.

### Effect of sequence hydrophobicity at positions 19 and 20

Double mutants at positions 19 and 20 with F<sub>5</sub>-Phe and Cha had an apparent additive effect on kinetics and thermodynamics of self-assembly. The double mutants display the same increased rate of self-assembly as was observed in the single mutants. The F<sub>5</sub>-Phe19,20 (8) and Cha19,20 (9) double mutants undergo complete fibril self-assembly to equilibrium within 30 min, making the relative rates impossible to differentiate using HPLC sedimentation

**Table 2** Critical concentrations and free energies for self-assembly of A $\beta$ (16–22) position 19 and position 20 variants

Peptide	Sequence	$C_r/\mu\text{M}$	$\Delta G/\text{kcal mol}^{-1}$	$\Delta\Delta G/\text{kcal mol}^{-1}$
1	Ac-KLVFFAE-NH <sub>2</sub>	$33 \pm 3$	$-6.4 \pm 0.1$	—
2	Ac-KLVFAAE-NH <sub>2</sub>	> 100	—	—
3	Ac-KLVYFAE-NH <sub>2</sub>	> 100	—	—
4	Ac-KLV(F <sub>5</sub> -Phe)FAE-NH <sub>2</sub>	$4 \pm 1$	$-7.7 \pm 0.1$	$-1.3 \pm 0.1$
5	Ac-KLV(Cha)FAE-NH <sub>2</sub>	$44 \pm 3$	$-6.2 \pm 0.1$	$0.2 \pm 0.1$
6	Ac-KLVF(F <sub>5</sub> -Phe)AE-NH <sub>2</sub>	$7 \pm 1$	$-7.3 \pm 0.1$	$-0.9 \pm 0.1$
7	Ac-KLVF(Cha)AE-NH <sub>2</sub>	$22 \pm 1$	$-6.6 \pm 0.1$	$-0.2 \pm 0.1$
8	Ac-KLV(F <sub>5</sub> -Phe)(F <sub>5</sub> -Phe)AE-NH <sub>2</sub>	$1 \pm 1$	$-8.5 \pm 0.1$	$-2.1 \pm 0.1$
9	Ac-KLV(Cha)(Cha)AE-NH <sub>2</sub>	$32 \pm 2$	$-6.4 \pm 0.1$	$0 \pm 0.1$

assays. Thermodynamically, the stabilization effects of the individual mutations appear to be additive. The F<sub>5</sub>-Phe19,20 variant shows a lower mean C<sub>r</sub> value than the F<sub>5</sub>-Phe19 mutant (1 ± 1 μM), indicating that the increased hydrophobicity caused by the F<sub>5</sub>-Phe substitution at position 20 further stabilizes the already substantially stabilized F<sub>5</sub>-Phe19 mutant fibrils relative to the wild-type ( $\Delta\Delta G = -2.1 \pm 0.1 \text{ kcal mol}^{-1}$ ). Similarly, the addition of a Cha residue at position 20 rescues the destabilizing effect of the Cha substitution at position 19 in the case of Cha19,20, resulting in fibrils as stable as wild-type fibrils (C<sub>r</sub> = 32 ± 1 μM,  $\Delta\Delta G = 0 \pm 0.1 \text{ kcal mol}^{-1}$ ). Once again, monomer dissociation from suspended fibrils confirmed these C<sub>r</sub> values (1 μM for F<sub>5</sub>-Phe19,20, 31 μM for Cha19,20, Fig. S1, ESI†).

### TEM imaging of fibrillar aggregates

Negatively stained (uranyl acetate) TEM images clearly show ordered fibrils several μm in length for all variants that were competent to self-assemble at starting concentrations of 55 μM (Fig. 3). The wild-type displayed twisted fibers consisting of smaller fibrils with an average diameter of 12 ± 0.3 nm; the individual fibrils that compose these fiber structures were not sufficiently resolved to determine diameters confidently. Twisted fibers were also displayed by the Cha19 peptide, with diameters of 14 ± 0.4 nm. The fibril morphology observed in the F<sub>5</sub>-Phe19 peptide consists of fiber bundles that were 20 ± 1 nm in diameter; these fibers consist of bundled, intertwined fibrils. The smallest fibrillar subunits that are clearly resolved within the bundles are 10.0 ± 0.5 nm in diameter. Similar twisted bundles with width of up to 30 nm were observed for the Cha20 mutant, however here the smallest fibrillar subunit observed was measured to be 5.0 ± 0.2 nm. F<sub>5</sub>-Phe20 showed well defined fibrils with diameters of 10.1 ± 0.2 nm. Both double mutants, Cha19,20 and F<sub>5</sub>-Phe19,20, showed well-defined fibrils. The diameter of fibers derived from F<sub>5</sub>-Phe19,20 was measured to be 13.0 ± 0.2 nm. The Cha19,20 variant did not display the common twisted fiber morphology, but rather a stiff tubular shape with strongly defined edges with a diameter of 10.0 ± 0.3 nm.

### X-Ray diffraction analysis of fibrils

Fibrils were harvested by centrifugation. The fibrillar pellets were washed repeatedly with water to remove buffer salts and the resulting material was dried and lyophilized. This material was subjected to X-ray powder diffraction analysis in order to confirm the characteristic amyloid diffraction pattern (Fig. 4). All variants show a distinct scattering intensity at angles corresponding to 4.7 Å, which are typical interstrand peptide–peptide spacings with β-sheets for cross-β fibrils. Strong β-sheet lamellar scattering intensities were only observed for Cha19, F<sub>5</sub>-Phe20 and both double mutants, which indicate some heterogeneity in terms of lamellar packing of β-sheets within fibrils. Under similar conditions, Aβ(16–22) fibrils are known to have lamellar spacings of ~10.1 Å, but it has been reported that these scattering intensities are sometimes weak or negligible.<sup>43</sup> The lamellar spacing of Cha19 fibrils was found to be ~10.9 Å, and may indicate that the larger side chain of Cha increases lamination distances.

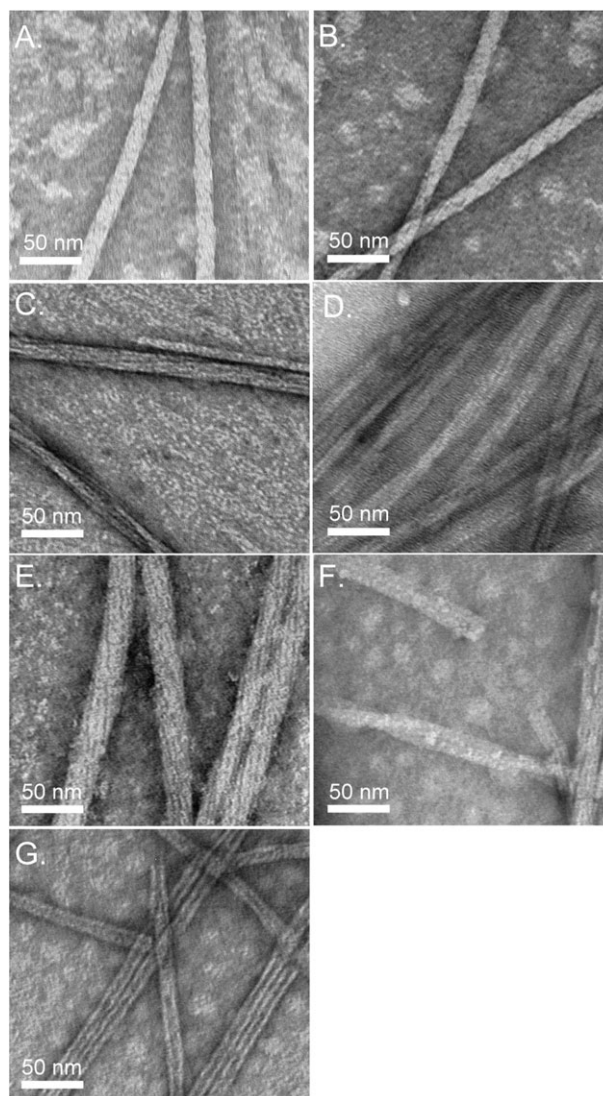


**Fig. 3** Negatively stained TEM images of fibrils derived from Aβ(16–22) variants. (A) Wild-type Aβ(16–22); (B) Phe19 → F<sub>5</sub>-Phe Aβ(16–22); (C) Phe19 → Cha Aβ(16–22); (D) Phe20 → F<sub>5</sub>-Phe Aβ(16–22); (E) Phe20 → Cha Aβ(16–22); (F) Phe19,20 → F<sub>5</sub>-Phe Aβ(16–22); (G) Phe19,20 → Cha Aβ(16–22).

Lamellar scatterings for F<sub>5</sub>-Phe20 and 19,20 fibrils were measured to be 9.3 and 9.9 Å, respectively, indicating tighter lamination.

### Secondary structure and determination of interstrand peptide packing registry by isotope-edited Fourier transform infrared spectroscopy (IE-IR)

FTIR spectra of fibrils of all variants show strong amide I stretches at ~1624 cm<sup>-1</sup> with weak stretches at ~1690 cm<sup>-1</sup> (Fig. 5A), indicative of an antiparallel β-sheet structure.<sup>39,43</sup> IE-IR was utilized to probe possible differences in intrasheet peptide packing orientations. IE-IR has been used to confirm peptide packing registry in amyloid peptide fibrils,<sup>54,55</sup> including Aβ(16–22).<sup>39,43,56</sup> In principle, specific incorporation of <sup>13</sup>C at the carbonyl of amino acids in the context of peptides results in a shift of the amide I stretch of the

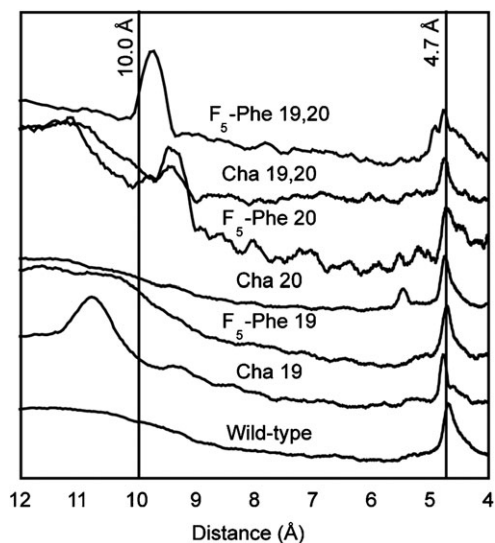


Fig. 4 X-Ray diffraction data from fibrils of A $\beta$ (16–22) variants.

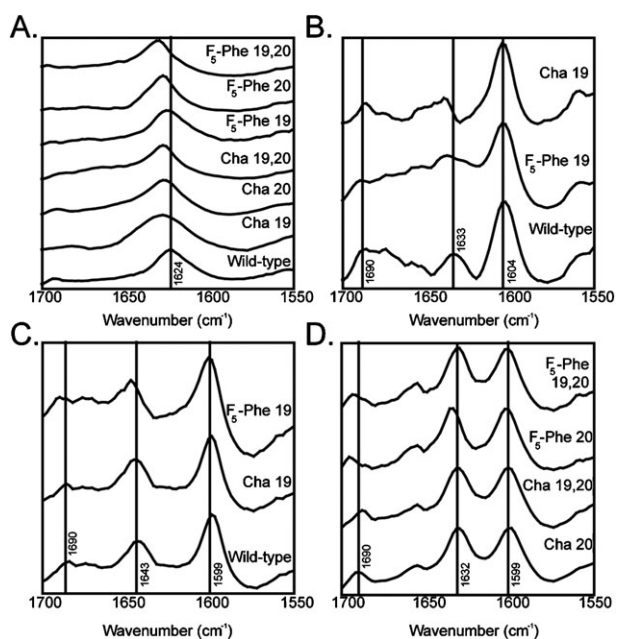


Fig. 5 IR spectra, including isotope-edited spectra, of fibrils derived from: (A) Unlabeled A $\beta$ (16–22) variants. (B) Double labeled with ( $1\text{-}^{13}\text{C}$ ) Leu17 and ( $1\text{-}^{13}\text{C}$ ) Ala21 A $\beta$ (16–22) variants (uncoupled). (C) Double labeled with ( $1\text{-}^{13}\text{C}$ ) Leu17 and ( $1\text{-}^{13}\text{C}$ ) Phe20 A $\beta$ (16–22) variants (coupled). (D) Double labeled with ( $1\text{-}^{13}\text{C}$ ) Lys16 and ( $1\text{-}^{13}\text{C}$ ) Ala21 A $\beta$ (16–22) variants (coupled).

labeled residue due to the lower vibrational frequency of  $^{13}\text{C}$  relative to  $^{12}\text{C}$ .<sup>54,57,58</sup> For example, in the context of A $\beta$ (16–22) fibrils, a shift from  $1624\text{ cm}^{-1}$  to  $1604\text{ cm}^{-1}$  is commonly observed at the labeled residue if the labeled amino acid is not in close proximity through space to other  $^{13}\text{C}$ -labeled residues. If the  $^{13}\text{C}$  labeled C=O is spatially adjacent to another  $^{13}\text{C}$  carbonyl, this shift can be further exaggerated due to coupling of these lower frequency vibrators. In the case of A $\beta$ (16–22) a shift to  $1599\text{ cm}^{-1}$  is observed when  $^{13}\text{C}$ -labeled amino acids are in close proximity (as opposed to  $1604\text{ cm}^{-1}$ ) facilitating

reasonably precise determination of peptide packing registry within the context of fibrillar architectures.<sup>39,43</sup>

Based on previous reports of fibrils derived from A $\beta$ (16–22), we expected that the packing register within variant fibrils would be antiparallel, in-register as shown in Fig. 6A and B.<sup>35,39,43</sup> This packing registry is favored at neutral pH due to complementary placement of charged Lys and Glu side chains between neighboring peptides within the  $\beta$ -sheet. In the antiparallel, in-register packing mode, the Phe19 side chain packs against Phe19 across  $\beta$ -strands, while the Phe20 phenyl group interacts with the side chain of Val18 residues. Recent molecular dynamics simulations have supported this preferred strand registry at neutral pH. Lynn *et al.* have shown that alternative packing modes within A $\beta$ (16–22)-derived amyloid

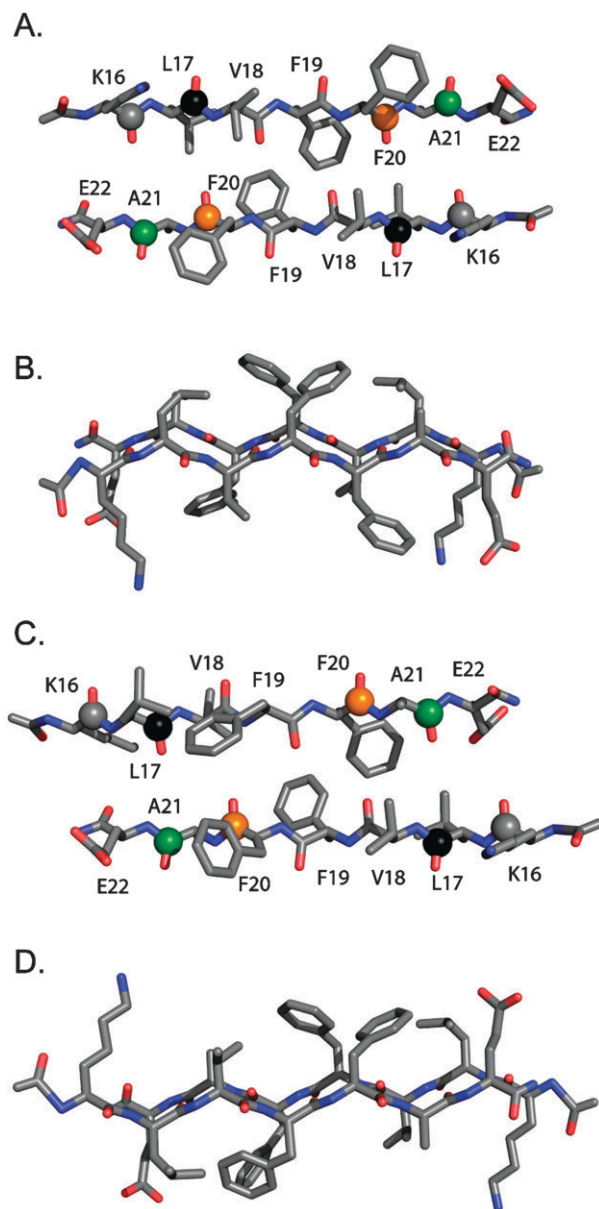


Fig. 6 Packing models for A $\beta$ (16–22). (A) Side view, antiparallel in-register orientation. (B) Top down view, antiparallel in register orientation. (C) Side view, out-of-register, flipped orientation. (D) Top down view, out-of-register, flipped orientation.

structures are possible as a function of pH.<sup>39,43</sup> At acidic pH, an antiparallel packing mode that involves an out-of-register shift in one peptide and a flip in its orientation places the side chains of Phe19 and Phe20 into an interactive relationship (Fig. 6C and D). This alternative strand-packing mode has been proposed to perturb laminar packing effects, limiting lamination to a bilayer that results in the observed nanotube morphology. In contrast, the common fibril morphology in A $\beta$ (16–22) fibrils involves the lamination of five  $\beta$ -sheets.<sup>39,43</sup> We hypothesized that the F<sub>5</sub>-Phe19 variant could possibly enforce this alternative packing mode, since it would place the complementary quadrupoles of F<sub>5</sub>-Phe19 and Phe20 into contact due to enhanced thermodynamic stability for F<sub>5</sub>-Phe–Phe interactions relative to Phe–Phe aromatic interactions.<sup>59</sup> To understand the implications of the observations reported herein, any possible changes in packing mode within the variant fibrils must be understood. In order to directly probe intrasheet packing orientations for peptides within fibrils derived from all variants, IE-IR studies were initiated.

<sup>13</sup>C-Labeling patterns for the Phe19, F<sub>5</sub>-Phe19, and Cha19 peptides were chosen in order to illuminate coupled and uncoupled interactions in the fibril structures and to clearly elucidate peptide packing registry. Peptides that incorporate Leu17 and Phe20 <sup>13</sup>C-carbonyl labels were expected to show a coupled IR spectrum (shift to  $\sim 1599\text{ cm}^{-1}$ ) if the in-register, antiparallel mode is adopted (Fig. 6A and B). Conversely, Leu17 and Ala21 <sup>13</sup>C-carbonyl labeled peptides should be coupled in the IR spectrum if the out-of-register packing mode is in effect (Fig. 6C and D). Thus, the Phe19, F<sub>5</sub>-Phe19, and Cha19 sequences were synthesized with L17/F20 and L17/A21 <sup>13</sup>C C=O labels and these peptides were fibrillized and subjected to IR analysis. Fibrils from the unlabeled wild-type peptide (Fig. 5A) have an amide I shift of  $1624\text{ cm}^{-1}$ . The amide I for the L17/A21 labeled peptide is shifted to  $1604\text{ cm}^{-1}$  (uncoupled, Fig. 5B) while that of the L17/F20 labeled fibrils is shifted to  $1599\text{ cm}^{-1}$  (coupled, Fig. 5C). These data are consistent with work published by Lynn *et al.* for this sequence and is consistent with an antiparallel, in-register peptide packing mode within the fibrils (Fig. 6A).<sup>39,43</sup> Fibrils from the F<sub>5</sub>-Phe19 peptide showed identical IE-IR coupling patterns to the wild-type peptide (L17/F20  $1598\text{ cm}^{-1}$ , L17/A21  $1603\text{ cm}^{-1}$ ), indicating that the intrasheet peptide packing mode is antiparallel, in-register. Finally, the Cha19 variant fibrils are also antiparallel, in-register by IE-IR analysis (L17/F20  $1598\text{ cm}^{-1}$ , L17/A21  $1603\text{ cm}^{-1}$ ).

Alternative labeling patterns were used in the position 20 and double mutant peptides, as one of the coupling partners in these systems, Phe20, was substituted by nonnatural amino acids which were not commercially available as the <sup>13</sup>C-labeled isotope. Encouraged by the results for the position 19 mutants, we chose Lys16 and Ala21 as labeling sites, since the carbonyl functionality in these amino acids should also be coupled across strands within  $\beta$ -sheets, providing positive indicators for the antiparallel, in-register packing mode. In all cases, fibrils derived from the position 20 and double mutants showed isotope shifted bands of  $\sim 1599\text{ cm}^{-1}$ , indicating coupling between the <sup>13</sup>C labeled carbonyls (Fig. 5D). These

data allow us to conclude that hydrogen-bonding mediated peptide–peptide interactions within the fibrils are identical between these variants, and that differences in thermodynamic measurements by HPLC sedimentation do not arise from changes in fibril  $\beta$ -sheet self-assembly arrangements but can be traced to differences in side chain interaction energies, desolvation energies, and lamination effects.

## Discussion

Collectively, these data are consistent with a prominent role for the Phe–Phe motif in the self-assembly of A $\beta$ (16–22). Variation of the hydrophobic and aromatic character of this motif in A $\beta$ (16–22) results in clear kinetic and thermodynamic perturbation of self-assembly. While less hydrophobic variants (Ala19 and Tyr19) fail to undergo self-assembly altogether, increasing hydrophobicity has a distinct kinetic effect. All variants that are more hydrophobic than the wild-type peptide undergo complete self-assembly in  $< 1\text{ h}$ , whereas the wild-type peptide exhibits a notable lag phase followed by slow fibrillization over  $\sim 2$  weeks. A general kinetic enhancement of self-assembly as a function of sequence hydrophobicity is consistent with an initial hydrophobic collapse of a critical mass of peptide, facilitating nucleation of ordered fibril growth. Increasing the hydrophobicity of the sequence should enhance the driving force for this hydrophobic collapse into a putative intermolecular molten globule,<sup>60</sup> which is not dependent on the formation of highly ordered non-covalent interactions, but is facilitated by desolvation and burial of hydrophobic groups. Thus, the rapid rate of self-assembly for the Cha and F<sub>5</sub>-Phe variants relative to the wild-type is not unexpected.<sup>61</sup> One important effect of sequence hydrophobicity on peptide self-assembly is enhanced initiation (hydrophobic collapse followed by nucleation) of the process.

Thermodynamically, the free energy associated with self-assembly of these variants displayed differential effects. Replacing Phe19 with the highly hydrophobic Cha unexpectedly resulted in a slight destabilization ( $+0.2\text{ kcal mol}^{-1}$ ) of the free energy associated with self-assembly. Conversely, the F<sub>5</sub>-Phe19 peptide was significantly stabilized relative to the wild-type peptide ( $-1.3\text{ kcal mol}^{-1}$ ). There are several factors that may account for the unexpected destabilizing effect of the Cha substitution at the central 19 position. First, a lack of  $\pi$ – $\pi$  interactions may slightly destabilize the self-assembly of these peptides. Second, the side chains of Phe, F<sub>5</sub>-Phe, and Cha are not precisely isosteric. Molecular modeling of each of the side chain rings (C<sub>6</sub>H<sub>6</sub>, C<sub>6</sub>H<sub>12</sub>, C<sub>6</sub>F<sub>5</sub>H) reveals that cyclohexane (Cha) is the largest of the side chain rings ( $148\text{ \AA}^3$ ), followed by pentafluorobenzene (F<sub>5</sub>-Phe,  $139\text{ \AA}^3$ ) and benzene (Phe,  $117\text{ \AA}^3$ ). In addition, the cyclohexyl ring of Cha is not planar. Differences in molecular volume and structural orientation may lead to perturbed packing, which in turn may diminish the thermodynamic effect of increased hydrophobicity in the case of the Cha19 variant. We hypothesize that significant steric effects associated with the Cha–Cha cross-strand pairing destabilize these assemblies to some degree. Conversely, the Cha–Val cross-strand pairing in the Cha20 mutant is more

forgiving of the higher steric demand of the Cha side chain, facilitating the comparative thermodynamic stabilization in fibrils derived from this variant.

Eisenberg *et al.* have proposed a strong steric effect on the propensity of peptide sequences to form amyloid.<sup>62</sup> Specifically, the amyloidogenicity of a given sequence is based, in part, on amino acid side chains in self-complementary  $\beta$ -strands to be sterically accommodated in the “steric zipper” of the resulting cross- $\beta$  amyloid. Based on this supposition, the destabilizing effect of the Cha–Cha cross-strand interaction is hardly surprising. Interestingly, the Eisenberg group analyzed the amyloidogenicity of the A $\beta$ (15–20) sequence (QKLVFF) and predicted that the Phe19Ala mutant (QKLVAF) should form energetically stabilized amyloid relative to wild-type on the basis of more favorable steric accommodation of Ala in the steric zipper relative to Phe.<sup>62</sup> This is in contrast to the work reported herein that indicates that the Ala19 variant of A $\beta$ (16–22) does not fibrillize. The packing registry of A $\beta$ (15–20) and A $\beta$ (16–22) fibrils is possibly different, accounting for this inconsistency. It is also, possible, however, that Eisenberg’s model, which focuses on the energetics of the fibrillar products, neglects treatment of energetic constraints that determine nucleation effects. It should be noted that hydrophobicity plays an important role in amyloid formation for many sequences, but relatively non-hydrophobic peptides (for example, polyglutamines) are also competent in forming amyloid. For these non-hydrophobic sequences, there may be distinct mechanisms at play, and thus the work reported herein may not be universally applicable to all amyloid-forming sequences.

Further consideration of these results in the context of previous work directed at understanding the contributions of  $\pi$ – $\pi$  interactions in protein secondary structure stabilization is informative. Tatko and Waters have conducted seminal studies that support the notion that  $\pi$ – $\pi$  interactions are selective and stabilizing in cross-strand pairs in  $\beta$ -hairpin structures.<sup>19</sup> By comparing Cha–Cha, Cha–Phe, and Phe–Phe pairing in a model hairpin, Waters concludes that the preference for self-association of Phe–Phe is  $-0.55$  kcal mol<sup>-1</sup>. This effect is largely enthalpic, however, since Phe–Phe interactions elicit an entropic penalty relative to Cha–Cha or Cha–Phe pairings. Presumably, this is due to the conformational constraints that exist for the formation of  $\pi$ – $\pi$  interactions. When both enthalpy and entropy are accounted for, Waters’s studies indicate that the overall free energy of the Cha–Cha pairing is more favorable than the Phe–Phe pairing.<sup>19</sup> Later work by Nowick *et al.* using a different model system shows no preference for Phe–Phe cross-strand pairing relative to Cha–Cha or Cha–Phe pairings in an apparent contradiction to Waters’s work, although this may be attributed to fundamental differences in the model systems used.<sup>29</sup> The studies reported herein are consistent with Phe–Phe pairings having an overall energetic advantage of  $-0.2$  kcal mol<sup>-1</sup> relative to Cha–Cha pairings. This value is less than the  $-0.55$  kcal mol<sup>-1</sup> reported by Waters, and no information is yet available on the relative enthalpic and entropic contributions in our system. There may be a higher entropic penalty due to the high degree of organization inherent in an amyloid structure.

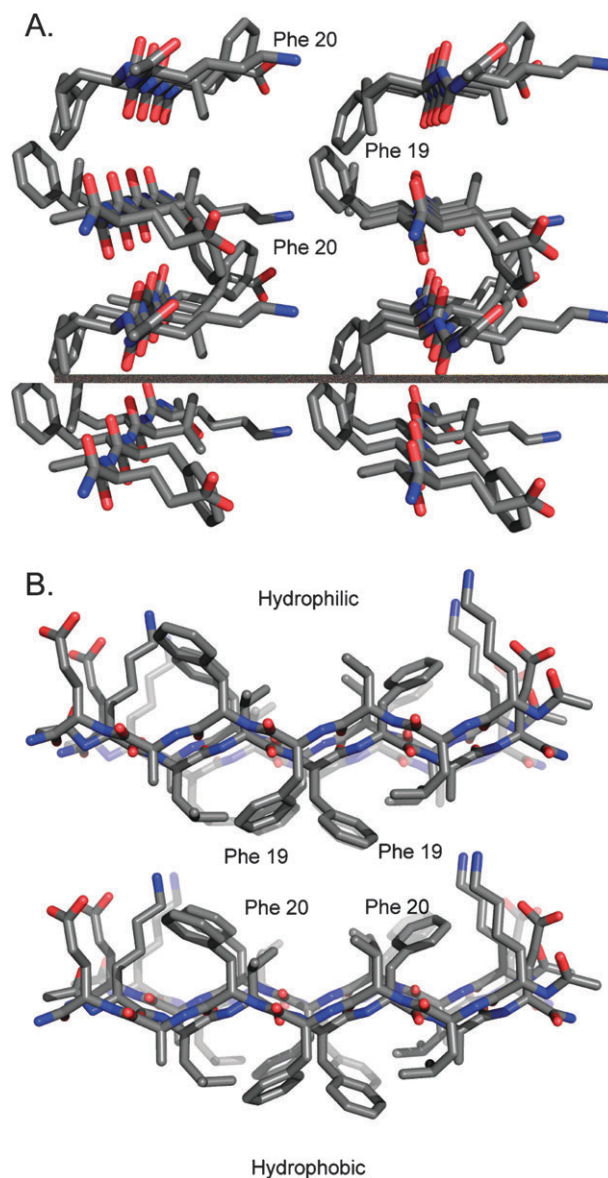


**Fig. 7** Model for lamination of two  $\beta$ -sheets within a fibril. Peptide–peptide hydrogen bonds, charge interactions, and hydrophobic/ $\pi$ – $\pi$  effects stabilize sheets. These same forces contribute to lamination of these sheets within the final fibrillar architecture.

Cross-strand contacts are not the only interactions perturbed by the mutations at positions 19 and 20, as both residues have been proposed to be involved in the lamination of  $\beta$ -sheets to form mature fibers (Fig. 7).<sup>35,39,42,43</sup> The current model indicates that the aromatic side chain of Phe19 may be involved in T-stacking  $\pi$ – $\pi$  interactions with cross-sheet Phe20 side chains, thus facilitating orientation specific lamination. An increase in hydrophobicity at positions 19 and 20 could enhance the lamination propensity as this process is driven by the burial of the hydrophobic face of the peptide monomer. Conversely, an increase in steric bulk or loss of  $\pi$ – $\pi$  interactions at either residue could negatively affect the lamination of the resulting sheet, leading to decrease in thermodynamic stability. The free energy differences measured herein undoubtedly reflect these interactions as

well. Recent work has indicated that residue 19 plays a more prominent role in lamination effects than residue 20 in the context of A $\beta$ (16–22) fibril formation,<sup>40</sup> and our results appear to be consistent with this contention.

The dramatic stabilization shown by F<sub>5</sub>-Phe–F<sub>5</sub>-Phe pairings (–1.3 kcal mol<sup>–1</sup> relative to Phe–Phe and –1.5 kcal mol<sup>–1</sup> relative to Cha–Cha) is interesting in this context as well. Previous work has shown that F<sub>5</sub>-Phe exerts significant effects in self-assembled systems.<sup>48</sup> F<sub>5</sub>-Phe is significantly more hydrophobic than Phe, but also possesses altered (nearly opposite) side chain quadrupole electronics relative to Phe. The dramatic stabilization of the F<sub>5</sub>-Phe–F<sub>5</sub>-Phe pairing may be a combination of aromatic/hydrophobic effects: aromatic interactions are consistent with the Phe–Phe pairing, but the high degree of hydrophobicity also imparts a significant energetic advantage. There is also a possibility that the strength of the aromatic  $\pi$ – $\pi$  interaction for the F<sub>5</sub>-Phe–F<sub>5</sub>-Phe pairing is greater relative to the Phe–Phe pairing as a function of side chain electronics. A third possibility is that fluorine interactions exert a significant influence in this system. It has been shown that highly fluorinated amino acids have a strong propensity to self-associate, and this may be a third energetic consideration in this case.<sup>63–65</sup> Fluorine effects in the context of F<sub>5</sub>-Phe have not been as heavily explored as those in aliphatic systems, including hexafluoroleucine.<sup>66–71</sup> While hexafluoroleucine appears to generally favor self-association in protein/peptide structures, this has not consistently been observed with F<sub>5</sub>-Phe. In some cases, F<sub>5</sub>-Phe prefers to associate with Phe in folded structures,<sup>47,72</sup> and this effect is nuanced by subtle electronic perturbation of the F<sub>5</sub>-Phe residues.<sup>73</sup> Based on this previous work, a blanket invocation of the “fluorous effect” to explain the observed increase in stability of the F<sub>5</sub>-Phe fibrils may be an oversimplification.

The  $\beta$ -sheet propensity of these amino acids should also be considered. Both Cha and F<sub>5</sub>-Phe have been shown to have enhanced  $\beta$ -sheet propensities relative to Phe<sup>19,74</sup> and Ala and Tyr are less prone to be found in  $\beta$ -sheet structures. The energetic stabilization of Phe–Phe *vs.* Cha–Cha cross-strand interactions may, in fact, be underestimated in this work as a function of the increased sheet propensity of Cha compared to Phe. Secondary structure propensities are undoubtedly reflected in the measured  $\Delta G$  values to some degree. The exact energetic contributions of hydrophobic effects,  $\pi$ – $\pi$  interactions, fluorine effects, steric interactions, and secondary structure propensity are exceedingly difficult to differentiate, and each of these biophysical parameters may exert significant influence during self-assembly processes.

## Conclusion

The biophysical determinants for peptide amyloidogenicity are complex. While there has been debate concerning the importance of specific aromatic  $\pi$ – $\pi$  interactions in peptide self-assembly processes, it is difficult to design systems that specifically measure the value of a  $\pi$ – $\pi$  interaction in the context of amyloid formation. Changing the aromaticity of a single amino acid (for example Phe  $\rightarrow$  Cha) inevitably also changes other properties of the amino acid, including sheet propensity, hydrophobicity, and exposed surface area. The

studies described herein are consistent with the formation of  $\pi$ – $\pi$  cross-strand interactions at position 19 in A $\beta$ (16–22) fibrils, but the exact energetic contribution of this interaction is exceedingly difficult to differentiate from hydrophobic desolvation effects or steric penalties. Expanded studies with A $\beta$ (16–22) and other amyloid systems will provide additional insight into the energetic determinants of peptide self-assembly. This insight will facilitate the advanced design of amyloid-derived materials and inform efforts to otherwise perturb these processes.

## Experimental

### Materials

All amino acids and solvents were obtained commercially and used without further purification. Water was purified by filtration to 18 m $\Omega$  purity.

### Peptide synthesis and purification

Peptides were synthesized using standard Fmoc peptide synthesis protocols on Rink amide resin with HBTU/HOBt activation. The N-terminal amine was acetylated and the peptide was cleaved from resin using a solution of TFA : H<sub>2</sub>O (99 : 1 v/v). The cleavage cocktail was reduced in volume and the peptide was precipitated by addition to diethyl ether. The precipitate was collected by centrifugation and the pellet was washed three times with diethyl ether. The pellet was dissolved in DMSO and purified by reverse-phase HPLC (Shimadzu, Waters XBridge™ BEH300 Prep C18 10 mM column) with a linear gradient of acetonitrile and water (0.1% TFA) (see ESI†). Peptide identity was confirmed using ESI or MALDI mass spectroscopy.

### Peptide disaggregation protocol

The purified peptides were disaggregated using a modified Wetzel protocol.<sup>49</sup> Briefly, the peptides were dissolved in TFA and sonicated for 10 min at room temperature. The TFA was removed under a gentle stream of dry nitrogen. The resulting film was immediately dissolved in HFIP and the solution was incubated at 37 °C for 2 h. The HFIP was removed under a gentle stream of dry nitrogen and the film was again dissolved in HFIP. The peptide concentration of this HFIP solution was determined by correlation to an HPLC concentration curve (see ESI† for details on the construction of concentration curves) and the desired amount of peptide was distributed into individual glass vials. The HFIP was again removed under a stream of dry nitrogen and the peptides were dried under vacuum for 16 h to remove residual HFIP. Dissolution of these peptides in DMSO followed by light scattering analysis confirmed the monomeric state of these peptides.

### Sedimentation assay

Sedimentation assays were executed by adapting the protocol of Wetzel *et al.*<sup>49</sup> The disaggregated peptides were dissolved in DMSO and diluted into the desired volume of phosphate buffered saline (137 mM NaCl, 2.7 mM KCl, 10 mM Na<sub>2</sub>HPO<sub>4</sub>, 1.8 mM KH<sub>2</sub>PO<sub>4</sub>, pH 7.4, 0.1% Na<sub>3</sub>N w/v;

DMSO was 5% by volume of the final solution). Concentrations were determined by correlation to HPLC concentration curves calibrated by amino acid analysis. Samples were incubated at 37 °C and aliquots were removed at predetermined times. These aliquots were centrifuged (350 000 g, 1 h, 4 °C) to remove fibrillar and oligomeric aggregates. The concentration of monomeric peptide in the supernatant was determined by correlation to HPLC calibration curves (see ESI†). The experimental equilibrium endpoint was determined as the point at which [peptide monomer] did not decrease after four consecutive data points. Peptide monomer concentrations remained unchanged once endpoint was reached, even after 4 weeks (data not shown). The critical concentration,  $C_r$ , is defined as the concentration of monomer peptide at endpoint and is reflective of the dynamic equilibrium between fibril and monomer.  $C_r$  is related to the association constant,  $K_a$ , for the addition of one additional molecule of monomeric peptide to a growing fibril. The association constant  $K_a$  (eqn (1)) can be derived from  $C_r$  as shown in eqn (2).<sup>49</sup>  $K_a$  values were used to calculate  $\Delta G$  values for each variant. All data points are the average of at least 3 replications and error is reported as the standard deviation of the mean.

$$K_a = \frac{[\text{fibril}_{n+1}]}{[\text{fibril}_n][\text{monomer}]} \quad (1)$$

$$K_a = \frac{1}{C_r} \quad (2)$$

Complete sedimentation of all aggregate structures by ultracentrifugation was confirmed by dynamic light scattering analysis (data not shown) of the supernatant, which showed no evidence of higher order structures. Reversibility of the self-assembly was investigated by reverse sedimentation assays: mature lyophilized fibrils were suspended in phosphate buffered saline solution (5% DMSO) and incubated at 37 °C. At set time intervals an aliquot was centrifuged to remove fibrils and the re-appearance of peptide monomer followed by analytical HPLC until critical concentration was reached (Fig. S1, ESI†).

### Transmission electron microscopy (TEM)

After each assembly reaction had reached the endpoint, 10  $\mu\text{L}$  aliquots of the solution were applied to TEM grids (carbon film coated copper, 200 mesh; Electron Microscopy Sciences, Hatfield, PA) and allowed to adsorb for 1 min. The excess peptide solution was removed using capillary action and the adsorbed fibrils were washed four times with water to remove residual salt and buffer. The grids were then stained with 10  $\mu\text{L}$  of 5% uranyl acetate for 3 min and the excess staining solution was removed *via* capillary action. The grids were allowed to air dry for 10 min. Images were recorded on a Hitachi 7650 transmission electron microscope in high contrast mode with an accelerating voltage of 80 kV. Fibril width was determined by performing at least 100 measurements on unique fibrils for each diameter using the program ImageJ (<http://rsbweb.nih.gov/ij/>).

### X-Ray diffraction (XRD)

Mature fibrils were harvested by centrifugation, washed with water, flash-frozen, and lyophilized. Powder diffraction measurements were performed on a Bruker X8 APEX II X-ray diffractometer.

### Fourier transform infrared spectroscopy (FTIR)

Fibrils were harvested as described above. The lyophilized powder was mixed with spectroscopy grade KBr crystals and pressed into a pellet. The pellet was analyzed on a Shimadzu FTIR-8400S spectrometer operating at a 4  $\text{cm}^{-1}$  resolution.

### Acknowledgements

We thank Karen Bentley at the University of Rochester URM Electron Microscope Research Core and Maura Weathers at the Cornell University CCMR X-ray facilities for technical assistance. We also acknowledge the Alzheimer's Association (NIRG-08-90797) and DuPont (Young Professor Award to BLN) for generous funding of this project. Mass spectroscopy instrumentation was supported, in part, by a grant from the U.S. National Science Foundation (CHE-0840410).

### References

- 1 F. Chiti and C. M. Dobson, *Annu. Rev. Biochem.*, 2006, **75**, 333–366.
- 2 F. Chiti and C. M. Dobson, *Nat. Chem. Biol.*, 2009, **5**, 15–22.
- 3 J. W. Kelly and W. E. Balch, *J. Cell Biol.*, 2003, **161**, 461–462.
- 4 S. K. Maji, M. H. Perrin, M. R. Sawaya, S. Jessberger, K. Vadodaria, R. A. Rissman, P. S. Singru, K. P. R. Nilsson, R. Simon, D. Schubert, D. Eisenberg, J. Rivier, P. Sawchenko, W. Vale and R. Riek, *Science*, 2009, **325**, 328–332.
- 5 K. Rajagopal and J. P. Schneider, *Curr. Opin. Struct. Biol.*, 2004, **14**, 480–486.
- 6 R. Langer and D. A. Tirrell, *Nature*, 2004, **428**, 487–492.
- 7 X. Zhao and S. Zhang, *Chem. Soc. Rev.*, 2006, **35**, 1105–1110.
- 8 I. Cherny and E. Gazit, *Angew. Chem., Int. Ed.*, 2008, **47**, 4062–4069.
- 9 R. V. Ulijn and A. M. Smith, *Chem. Soc. Rev.*, 2008, **37**, 664–675.
- 10 J. P. Jung, J. Z. Gasiorowski and J. H. Collier, *Biopolymers*, 2010, **94**, 49–59.
- 11 M. Bartolini and V. Andrisano, *ChemBioChem*, 2010, **11**, 1018–1035.
- 12 F. Bemporad, G. Calloni, S. Campioni, G. Plakoutsi, N. Taddei and F. Chiti, *Acc. Chem. Res.*, 2006, **39**, 620–627.
- 13 I. W. Hamley, *Angew. Chem., Int. Ed.*, 2007, **46**, 8128–8147.
- 14 O. S. Makin, E. Atkins, P. Sikorski, J. Johansson and L. C. Serpell, *Proc. Natl. Acad. Sci. U. S. A.*, 2005, **102**, 315–320.
- 15 F. Chiti, M. Stefani, N. Taddei, G. Ramponi and C. M. Dobson, *Nature*, 2003, **424**, 805–808.
- 16 M. L. Waters, *Curr. Opin. Chem. Biol.*, 2002, **6**, 736–741.
- 17 E. Gazit, *FASEB J.*, 2002, **16**, 77–83.
- 18 S. M. Butterfield, P. R. Patel and M. L. Waters, *J. Am. Chem. Soc.*, 2002, **124**, 9751–9755.
- 19 C. D. Tatko and M. L. Waters, *J. Am. Chem. Soc.*, 2002, **124**, 9372–9373.
- 20 G. W. Platt, K. E. Routledge, S. W. Homans and S. E. Radford, *J. Mol. Biol.*, 2008, **378**, 251–263.
- 21 R. Azriel and E. Gazit, *J. Biol. Chem.*, 2001, **276**, 34156–34161.
- 22 D. Zanuy, Y. Porat, E. Gazit and R. Nussinov, *Structure*, 2004, **12**, 439–455.
- 23 A. Frydman-Marom, M. Rechter, I. Shefler, Y. Bram, D. E. Shalev and E. Gazit, *Angew. Chem., Int. Ed.*, 2009, **48**, 1981–1986.
- 24 Y. Porat, Y. Mazar, S. Efrat and E. Gazit, *Biochemistry*, 2004, **43**, 14454–14462.

- 25 Y. Porat, A. Abramowitz and E. Gazit, *Chem. Biol. Drug Des.*, 2006, **67**, 27–37.
- 26 T. Cohen, A. Frydman-Marom, M. Rechter and E. Gazit, *Biochemistry*, 2006, **45**, 4727–4735.
- 27 S. M. Tracz, A. Abedini, M. Driscoll and D. P. Raleigh, *Biochemistry*, 2004, **43**, 15901–15908.
- 28 P. Marek, A. Abedini, B. Song, M. Kanungo, M. E. Johnson, R. Gupta, W. Zaman, S. S. Wong and D. P. Raleigh, *Biochemistry*, 2007, **46**, 3255–3261.
- 29 D. M. Chung, Y. Dou, P. Baldi and J. S. Nowick, *J. Am. Chem. Soc.*, 2005, **127**, 9998–9999.
- 30 F. Bemporad, N. Taddei, M. Stefani and F. Chiti, *Protein Sci.*, 2006, **15**, 862–870.
- 31 A. P. Pawar, K. F. Dubay, J. Zurdo, F. Chiti, M. Vendruscolo and C. M. Dobson, *J. Mol. Biol.*, 2005, **350**, 379–392.
- 32 C. H. Gorbitz, *Chem.–Eur. J.*, 2001, **7**, 5153–5159.
- 33 M. Reches and E. Gazit, *Science*, 2003, **300**, 625–627.
- 34 M. Reches and E. Gazit, *Amyloid*, 2004, **11**, 81–89.
- 35 J. J. Balbach, Y. Ishii, O. N. Antzutkin, R. D. Leapman, N. W. Rizzo, F. Dyda, J. Reed and R. Tycko, *Biochemistry*, 2000, **39**, 13748–13759.
- 36 K. Lu, J. Jacob, P. Thiyagarajan, V. P. Conticello and D. G. Lynn, *J. Am. Chem. Soc.*, 2003, **125**, 6391–6393.
- 37 S. Santini, G. Wei, N. Mousseau and P. Derreumaux, *Structure*, 2004, **12**, 1245–1255.
- 38 T. Takeda and D. K. Klimov, *J. Mol. Biol.*, 2007, **368**, 1202–1213.
- 39 A. K. Mehta, K. Lu, W. S. Childers, Y. Liang, S. N. Dublin, J. Dong, J. P. Snyder, S. V. Pingali, P. Thiyagarajan and D. G. Lynn, *J. Am. Chem. Soc.*, 2008, **130**, 9829–9835.
- 40 H. Inouye, K. A. Gleason, D. Zhang, S. M. Decatur and D. A. Kirschner, *Proteins*, 2010, **78**, 2306–2321.
- 41 J. A. Wallace and J. K. Shen, *Biochemistry*, 2010, **49**, 5290–5298.
- 42 A. T. Petkova, G. Buntkowsky, F. Dyda, R. D. Leapman, W. M. Yau and R. Tycko, *J. Mol. Biol.*, 2004, **335**, 247–260.
- 43 Y. Liang, S. V. Pingali, A. S. Jogalekar, J. P. Snyder, P. Thiyagarajan and D. G. Lynn, *Biochemistry*, 2008, **47**, 10018–10026.
- 44 M. Suzuki, T. Takahashi, J. Sato, M. Mie, E. Kobatake and H. Mihara, *ChemBioChem*, 2010, **11**, 1525–1530.
- 45 J. L. Fauchère, M. Charton, L. B. Kier, A. Verloop and V. Pliska, *Int. J. Pept. Protein Res.*, 1988, **32**, 269–278.
- 46 C. J. Bowerman, D. M. Ryan, D. A. Nissan and B. L. Nilsson, *Mol. BioSyst.*, 2009, **5**, 1058–1069.
- 47 M. G. Woll, E. B. Hadley, S. Mecozzi and S. H. Gellman, *J. Am. Chem. Soc.*, 2006, **128**, 15932–15933.
- 48 D. M. Ryan, S. B. Anderson, F. T. Senguen, R. E. Youngman and B. L. Nilsson, *Soft Matter*, 2010, **6**, 475–479.
- 49 B. O’Nuallain, A. K. Thakur, A. D. Williams, A. M. Bhattacharyya, S. Chen, G. Thiagarajan and R. Wetzel, *Methods Enzymol.*, 2006, **413**, 34–74.
- 50 W. S. Childers, A. K. Mehta, K. Lu and D. G. Lynn, *J. Am. Chem. Soc.*, 2009, **131**, 10165–10172.
- 51 M. J. Krysmann, V. Castelletto, A. Kelarakis, I. W. Hamley, R. A. Hule and D. J. Pochan, *Biochemistry*, 2008, **47**, 4597–4605.
- 52 L. O. Tjernberg, D. J. E. Callaway, A. Tjernberg, S. Hahne, C. Lilliehöök, L. Terenius, J. Thyberg and C. Nordstedt, *J. Biol. Chem.*, 1999, **274**, 12619–12625.
- 53 A. D. Williams, S. Shivaprasad and R. Wetzel, *J. Mol. Biol.*, 2006, **357**, 1283–1294.
- 54 H. Hiramatsu and T. Kitagawa, *Biochim. Biophys. Acta*, 2005, **1753**, 100–107.
- 55 S. M. Decatur, *Acc. Chem. Res.*, 2006, **39**, 169–175.
- 56 S. A. Petty and S. M. Decatur, *J. Am. Chem. Soc.*, 2005, **127**, 13488–13489.
- 57 J. Kubelka and T. A. Keiderling, *J. Am. Chem. Soc.*, 2001, **123**, 12048–12058.
- 58 C. Paul and P. H. Axelsen, *J. Am. Chem. Soc.*, 2005, **127**, 5754–5755.
- 59 S. Mecozzi, A. P. West, Jr. and D. A. Dougherty, *Proc. Natl. Acad. Sci. U. S. A.*, 1996, **93**, 10566–10571.
- 60 Y. Liang, D. G. Lynn and K. M. Berland, *J. Am. Chem. Soc.*, 2010, **132**, 6306–6308.
- 61 A. D. Williams, E. Portelius, I. Kheterpal, J. T. Guo, K. D. Cook, Y. Xu and R. Wetzel, *J. Mol. Biol.*, 2004, **335**, 833–842.
- 62 L. Goldschmidt, P. K. Teng, R. Riek and D. Eisenberg, *Proc. Natl. Acad. Sci. U. S. A.*, 2010, **107**, 3487–3492.
- 63 E. N. G. Marsh, *Chem. Biol.*, 2000, **7**, R153–R157.
- 64 N. C. Yoder and K. Kumar, *Chem. Soc. Rev.*, 2002, **31**, 335–341.
- 65 C. Jäckel, M. Salwiczek and B. Koksich, *Angew. Chem., Int. Ed.*, 2006, **45**, 4198–4203.
- 66 B. Bilgicer, A. Fichera and K. Kumar, *J. Am. Chem. Soc.*, 2001, **123**, 4393–4399.
- 67 Y. Tang, G. Ghirlanda, W. A. Petka, T. Nakajima, W. F. DeGrado and D. A. Tirrell, *Angew. Chem., Int. Ed.*, 2001, **40**, 1494–1496.
- 68 Y. Tang and D. A. Tirrell, *J. Am. Chem. Soc.*, 2001, **123**, 11089–11090.
- 69 K. H. Lee, H. Y. Lee, M. M. Slutsky, J. T. Anderson and E. N. G. Marsh, *Biochemistry*, 2004, **43**, 16277–16284.
- 70 H. P. Chiu, Y. Suzuki, D. Gullickson, R. Ahmad, B. Kokona, R. Fairman and R. P. Cheng, *J. Am. Chem. Soc.*, 2006, **128**, 15556–15557.
- 71 H. Y. Lee, K. H. Lee, H. M. Al-Hashimi and E. N. G. Marsh, *J. Am. Chem. Soc.*, 2006, **128**, 337–343.
- 72 G. Cornilescu, E. B. Hadley, M. G. Woll, J. L. Markley, S. H. Gellman and C. C. Cornilescu, *Protein Sci.*, 2007, **16**, 14–19.
- 73 H. Zheng, K. Comeforo and J. Gao, *J. Am. Chem. Soc.*, 2009, **131**, 18–19.
- 74 H. P. Chiu, B. Kokona, R. Fairman and R. P. Cheng, *J. Am. Chem. Soc.*, 2009, **131**, 13192–13193.